Desalination and Water Treatment
www.deswater.com

doi: 10.5004/dwt.2018.21865

104 (2018) 62–72
February

Enhanced anti-fouling property of poly(vinyl chloride) membrane by blending poly(*N*-acryloylmorpholine)-grafted ZrO_2 nanoparticle

Xiang Shen*, Tiande Xie, Jiangang Wang, Fan Wang

College of Chemistry and Environmental Science, Qujing Normal University, Qujing 655011, China, Tel./Fax: +86 874 8998658; emails: sx008100@163.com (X. Shen), 2819237151@qq.com (T. Xie), 993550313@qq.com (J. Wang), wfan321@126.com (F. Wang)

Received 3 August 2017; Accepted 30 December 2017

ABSTRACT

In this work, poly(*N*-acryloylmorpholine)-grafted ZrO_2 nanoparticles (ZrO_2-*g*-PACMO) were directly blended with poly(vinyl chloride) (PVC) to prepare a hybrid membrane via the phase inversion method. In addition, the effects of ZrO_2-*g*-PACMO and ZrO_2 nanoparticles on the structure and performance of resultant PVC membranes were comparatively investigated. The results indicated that the PVC/ZrO_2-*g*-PACMO membrane exhibited a large macroviod of cross-section and a rough membrane surface. During membrane formation, the hydrophilic PACMO chains were preferably enriched onto the membrane surface, leading to the enhancement of surface hydrophilicity and the reduction of adhesion force between protein and membrane surface. The amount of adsorbed bovine serum albumin (BSA) on the poly(vinylidene fluoride)/ZrO_2-*g*-PACMO decreases about 73% and 48% respectively, compared with original PVC and PVC/ZrO_2 membranes. Cycle filtration of pure water and BSA solution (0.5 g/L) confirmed that the total and irreversible membrane fouling were remarkably suppressed after incorporating ZrO_2-*g*-PACMO into PVC membrane. Although the original ZrO_2 nanoparticle was also found to improve the protein fouling resistance of PVC membrane, there was a fatal limitation that the original ZrO_2 exhibited an agglomeration tendency during the membrane formation. The outcomes of the present work demonstrate that the synthesized ZrO_2-*g*-PACMO nanoparticles have the potential for the design and preparation of anti-fouling PVC membrane.

Keywords: PVC; ZrO_2; Poly(*N*-acryloylmorpholine); Anti-fouling; Hybrid membrane

1. Introduction

Polymeric membranes have become more popular in the wastewater treatment, due to the favorable selectivity for particles, pathogens and organic substances in wastewater [1,2]. Despite the advantages of polymeric membranes, the membrane fouling is always induced by the deposition and/or adsorption of foulants on the surface, which significantly degrades the separation efficiency and shortens the service lifespan of membranes in wastewater treatment [3]. Therefore, it is necessary to modify the polymeric membrane to improve the anti-fouling property.

Among the polymeric materials, poly(vinyl chloride) (PVC) is broadly used to fabricate microfiltration (MF) and ultrafiltration (UF) membranes because it has the excellent stiffness, low cost and good mechanical strength [4]. The major drawback of PVC membranes is the hydrophobic nature, resulting in the serious membrane fouling in wastewater treatments [5,6]. Improving surface hydrophilicity of PVC membrane seems to be an effective way to suppress the membrane fouling. Several technologies have been proposed to increase the surface hydrophilicity of PVC membrane, such as the surface modification of membrane via coating or chemical grafting [7–9], and blending of hydrophilic additives [10–14]. Although the surface coating and chemical grafting layers significantly resist membrane fouling, extra

* Corresponding author.

steps are mandatory during the membrane modification process. More importantly, the surface pores of membranes can be blocked by the coating and grafting layers, resulting in the decrease of permeation flux [15]. During the membrane formation process, blending of hydrophilic additives in the casting solution exhibits an advantage that the desired structure and performance of resultant membranes can be obtained from the convenient operation and mild conditions of the phase inversion method [16].

Recently, the blending of inorganic nanoparticles has been proved effective in preparing hydrophilic membrane with the excellent anti-fouling property [17], and nanoparticles added to the membrane matrix have included SiO_2 [18,19], Al_2O_3 [20], ZnO [21] and TiO_2 [22–24]. For example, Rabiee et al. [21,22] reported on the fabrication of PVC/ZnO and PVC/TiO_2 nanocomposite UF membranes using a phase inversion method. The pure water flux and surface hydrophilicity of membranes increased with the increase of nanoparticles concentration in the casting solution. Similar experimental results were also obtained previously by Behboudi et al. [23] for PVC/TiO_2 membrane. Different from TiO_2, Al_2O_3 and ZnO nanoparticles, ZrO_2 may be more suitable to prepare hybrid membranes because of the excellent chemical stability [25]. Maximous et al. [26] fabricated poly(ethersulfone)/ZrO_2 (PES/ZrO_2) hybrid membranes, and found that the flux decline of membranes was significantly suppressed. Zheng et al. [27] reported that the introduction of ZrO_2 into poly(vinylidene fluoride) (PVDF) membrane was in favor of the improvement in the membrane surface hydrophilicity. Despite the numerous advantages of incorporating nanoparticles, the blending of nanoparticles in membrane matrix is restricted by the aggregation and agglomeration tendency [28].

The modification of nanoparticles using organic polymers is a feasible approach to enhance the dispersion stability of nanoparticles in membrane matrix [29]. Inspired by this typical characteristic, Liu et al. [30] grafted poly(methyl methacrylate) chains onto TiO_2 nanoparticles via atom transfer radical polymerization. The results showed that the modified nanoparticles were homogeneously dispersed into the PVDF matrix, and the prepared hybrid PVDF membrane exhibited the excellent anti-fouling property. Poly (*N*-acryloylmorpholine) (PACMO) has a wealth of hydrophilic polymer chains with a repellent resistant property for protein adsorption and cell adhesion [31–35]. In our previous work [36], the PACMO-grafted ZrO_2 nanoparticles (ZrO_2-*g*-PACMO) were synthesized via radical polymerization, followed by blending with PVDF to prepare hybrid membranes. The grafted PACMO chains can not only increase dispersion and stability of ZrO_2 nanoparticles in membrane matrix, but also enhance the hydrophilicity and oil/water separation efficiency of membrane. To the best of our knowledge, although some significant investigations have been conducted to prepare PVC membrane with nanoparticles as the additives, introducing polymer-grafted ZrO_2 nanoparticles to improve the anti-fouling property of PVC membrane is rarely reported.

In the present work, ZrO_2-*g*-PACMO nanoparticles are directly blended with PVC to fabricate hybrid membrane via the phase inversion method. In particular, the effects of polymer-grafted ZrO_2 and original ZrO_2 nanoparticles on the morphology, hydrophilicity, anti-fouling ability and permeation property of resultant membranes are comparatively investigated via X-ray photoelectron spectroscopy (XPS), scanning electron microscope (SEM), atom force microscopy (AFM), water contact angle measurement, protein adsorption and filtration experiments.

2. Experimental

2.1. Materials

PVC (M_w = 150,000) resin was supplied by Sekisui Chemical Co., Ltd. (Tokyo, Japan). Poly(ethylene glycol) (PEG, M_n = 20,000), *N*-acryloylmorpholine (ACMO), *N*,*N*-dimethylformamide (DMF), [3-(methacryloyloxy)propyl] trimethoxysilane (KH570), 2,2′-azobisisobutyronitrile (AIBN) and bovine serum albumin (BSA) were purchased from Xiyashiji Chemical Co., Ltd. (Shandong, China). ZrO_2 nanoparticles (average diameter = 50 nm) were supplied by Aladdin Reagent Co., Ltd. (Shanghai, China). The pure water (18 MΩ) used for all experiments was purified with a Milli-Q system (Millipore, America). All other chemicals, unless otherwise stated, were obtained from commercial sources and used as-received.

2.2. Synthesis and characterization of nanoparticles

The ZrO_2-*g*-PACMO nanoparticles were synthesized via radical copolymerization, and the detailed procedures were described in our previous work [36]. In brief, 2.5 g of ZrO_2 nanoparticles was ultrasonically dispersed in a mixture of ethanol (50 mL) and pure water (50 mL). 2.5 mL of KH570 was then added into the suspension. After the reaction was carried out under nitrogen atmosphere at 40°C for 5 h, the nanoparticles were collected by centrifugation and washed with ethanol to remove excess KH570. The resultant nanoparticles were denoted as ZrO_2-KH570. To synthesize the ZrO_2-*g*-PACMO nanoparticle, 1.5 g of ZrO_2-KH570 nanoparticles were immersed and then sonicated in 50 mL of ethanol for 30 min. After the suspension was bubbled with nitrogen for 20 min, 3.53 g of ACMO and 0.041 g of AIBN were introduced. The reaction was conducted at 60°C for 6 h. The nanoparticles were centrifuged (4,000 rpm, 15 min) and washed with ethanol, and dried under vacuum at 60°C for 24 h.

Fourier transform infrared spectroscopy (FTIR, Tensor37, Bruker, Germany) was used to determine the chemical structure of nanoparticles. Each spectrum was captured by averaged 32 scans at a resolution of 4 cm^{-1}.

Thermogravimetric analysis (TGA) of nanoparticles was conducted on a PerkinElmer Pyris 1 TGA instrument (USA) from room temperature to 1,000°C with a heating rate of 10°C/min under nitrogen atmosphere. The grafting amount of PACMO chains onto nanoparticles was calculated by following the previous descriptions [37].

Dispersion stability of nanoparticles was investigated via particle size distributions and sedimentation behaviors. 0.1 g of ZrO_2 or ZrO_2-*g*-PACMO nanoparticles was ultrasonically dispersed in 5 mL of DMF for 30 min. Particle size distributions of ZrO_2 or ZrO_2-*g*-PACMO nanoparticles in DMF solvent were tested via the nanoparticle size analyzer (Nano ZS90, Malvern). After the suspension was allowed to stand for 0, 12 and 24 h, respectively, the sedimentation behaviors of nanoparticles were also evaluated.

2.3. Preparation and characterization of membranes

The pristine PVC, PVC/ZrO_2 and PVC/ZrO_2-*g*-PACMO membranes were fabricated via the phase inversion method, and the compositions of casting solutions are listed in Table 1. Briefly, measured amount of nanoparticles was first immersed into DMF, followed by ultrasonication for 30 min to achieve homogenous suspension. PVC and PEG polymers were added into the suspension, and the solution was stirred for 6 h at 60°C to prepare the casting solution. After the air bubbles were released for 24 h, the casting solution was cast on a glass slide using a knife with a thickness of 300 μm. The liquid membrane was instantly immersed into a coagulation bath (25°C of pure water). After peeled off from the glass plate, the resultant membranes were completely washed with pure water to remove residual agents, and kept in pure water bath before use.

Viscosity measurements of the casting solutions were carried out on a R/S Rheometer (KINEXUS, Malvern, England) using a cone geometry. The temperature during the measurements was set to 25°C via a circulating water system. The prepared casting solution was placed onto a specimen stage, and viscosity was determined at 50 s^{-1} of shear rate.

XPS (PHI5000C ESCA system, PHI Co., USA) was utilized to characterize the elemental composition of the membrane surface. Survey spectra were measured at a take-off angle of 90° with respect to the sample surface using 300 W Al Kα radiation.

The cross-sectional and surface morphologies of the prepared membranes were observed using an SEM (Phenom Pro X, Netherland) at an acceleration voltage of 5.0 kV.

The overall porosity (ε) of a membrane sample was determined by the gravimetric method [38], as calculated by the following equation:

$$\varepsilon = \frac{w_1 - w_2}{A \times l \times \rho} \times 100\% \tag{1}$$

where w_1 and w_2 are the weights of the wet and dry membrane, respectively. A represents the membrane effective area (m^2), ρ is the water density and l denotes the membrane thickness (m).

The pore size distributions of membranes were evaluated by Kubo-X1000 analyzer (Beijing Builder Electronic Technology Co., Ltd., Beijing), which was derived from the nitrogen adsorption–desorption isotherms using the Barrett–Joyner–Halenda model [34]. The reported value was the average of three measurements.

The surface morphology of membranes was also scanned on an AFM (CSPM5500, Benyuan-nano, China). Membrane sample with a small square (2 cm × 2 cm) was loaded on a specimen stage before being scanned. The three-dimensional image was acquired from a scanning range of 10 μm × 10 μm. The mean roughness (R_a), root mean square (R_q) and mean difference in the height between the highest peaks and the lowest valleys (R_z) were studied by AFM software. The average of at least five scans was reported on each membrane. The interaction force between the membrane surface and BSA-immobilized tips was detected by AFM. BSA protein was chemically immobilized on the AFM tip using the procedures described elsewhere [39]. When the BSA-immobilized AFM tip approached to and/or retracted from the membrane surface, the cantilever deflection was generated due to the interaction force between the tip and membrane surface. By multiplying the spring constant of the cantilever, the interaction force could be calculated and thus a force-extension curve was collected.

The hydrophilicity of membranes was evaluated by measuring the pure water contact angle of the top surface. The contact angle change in the drop age was recorded using a contact angle instrument (DSA100, Krüss, Germany). 5 μL of water drop was dripped onto the membrane surface and the values of contact angle were obtained using the drop shape image analysis system.

The protein fouling resistance of the prepared membranes was evaluated using BSA adsorption. The membrane sample with a regular shape of 2 cm × 2 cm was immersed into 10 mL of BSA solution (1 g/L). After incubation at 25°C for 24 h to reach adsorption equilibrium, the amount (Q_p) of adsorbed protein was calculated by the following expression:

$$Q_p = \frac{(C_0 - C_1)V}{S} \tag{2}$$

where C_0 and C_1 are the initial and equilibrium BSA concentrations, respectively. S is the adsorption area of membrane sample and V is the volume of BSA solution. The concentrations of BSA solution before and after adsorption were determined by measuring the absorbance at 280 nm using the UV–vis spectrophotometer (UV-1601, Shimadzu, Japan).

2.4. Filtration experiments

The permeability and anti-fouling ability of the prepared membranes were characterized by filtration experiments at ambient temperature. A system described in the previous work was used for the filtration study [34]. Each membrane was initially compacted with pure water for 30 min at 0.2 MPa. The pure water flux at 0.2 MPa ($J_{w,1}$) was calculated by the following equation:

$$J = \frac{V}{A \times \Delta t} \tag{3}$$

where V (L) was the volume of permeated pure water. A (m^2) and Δt (h) represented the effective area of membrane and

Table 1
Compositions and viscosities of casting solutions

Membrane ID	PVC (g)	ZrO_2 (g)	ZrO_2-*g*-PACMO (g)	PEG (g)	DMF (g)	Viscosity (Pa·s)
PVC	8	–	–	2	50	0.85 ± 0.05
PVC/ZrO_2	7	1	–	2	50	0.46 ± 0.02
PVC/ZrO_2-*g*-PACMO	7	–	1	2	50	0.30 ± 0.03

permeation time, respectively. Subsequently, the pure water was replaced by 0.5 g/L of BSA solution. The BSA filtration was carried out at 0.2 MPa, and the flux (J_p) was obtained. Finally, the membrane was washed with pure water for 30 min and the pure water flux ($J_{w,2}$) was measured again. The rejection ratio during BSA filtration was calculated using Eq. (4):

$$R = \frac{C_f - C_p}{C_f} \times 100\% \quad (4)$$

where C_f and C_p are the concentration of BSA in the feed and permeate solution, respectively.

The flux recovery ratio (FR) represented the relative decline of pure water flux, which was used as the evaluation of protein fouling during filtration process. The FR values of membranes were calculated from Eq. (5):

$$\mathrm{FR} = \frac{J_{w,2}}{J_{w,1}} \times 100\% \quad (5)$$

To further analyze the fouling process in details, several membrane fouling ratios were defined. The total membrane fouling ratio (R_t) was calculated by Eq. (6):

$$R_t = \frac{J_{w,1} - J_p}{J_{w,1}} \times 100\% \quad (6)$$

R_r and R_{ir} were incorporated to distinguish reversible and irreversible fouling, which were defined by Eqs. (7) and (8), respectively.

$$R_r = \frac{J_{w,2} - J_p}{J_{w,1}} \times 100\% \quad (7)$$

$$R_{ir} = \frac{J_{w,1} - J_{w,2}}{J_{w,1}} \times 100\% \quad (8)$$

3. Results and discussions

3.1. Characterization of nanoparticles

The silane coupling agent KH570 was used to react with ZrO_2 nanoparticles to prepare the intermediate products (ZrO_2-KH570) with active C=C groups. Subsequently, ACMO monomers were grafted onto ZrO_2-KH570 to obtain the ZrO_2-*g*-PACMO nanoparticles via radical copolymerization. The chemical structure of the synthesized nanoparticles was investigated via FTIR spectra. As shown in Fig. 1(a), the spectrum of original ZrO_2 nanoparticles reveals a peak at 3,420 cm^{-1} that is associated with the stretching vibration of –OH groups. In the spectrum of ZrO_2-KH570, the bonds at 1,720 and 1,172 cm^{-1} are assigned to the O–C=O and C–O–C of KH570, respectively [40]. Compared with spectrum of ZrO_2-KH570, several new signals appear in the spectrum of ZrO_2-*g*-PACMO, namely C–O–C stretching vibration at 1,238 and 1,114 cm^{-1}, and C–N stretching vibration at 1,446 cm^{-1} of PACMO chains, respectively [35,36]. The FTIR spectra indicate that the PACMO chains have been grafted onto nanoparticle surface.

TGA analysis was used to characterize the thermal decomposition behaviors of nanoparticles, and the grafting amount of PACMO chains was quantitatively calculated according to the procedures described in the previous work [37]. Compared with ZrO_2 nanoparticles, Fig. 1(b) shows that the weight losses of ZrO_2-KH570 and ZrO_2-*g*-PACMO nanoparticles are about 0.78 and 1.46 wt%, respectively. Obviously, the relative weight loss of ZrO_2-*g*-PACMO nanoparticles is about 0.68 wt%, compared with ZrO_2-KH570. In another word, the

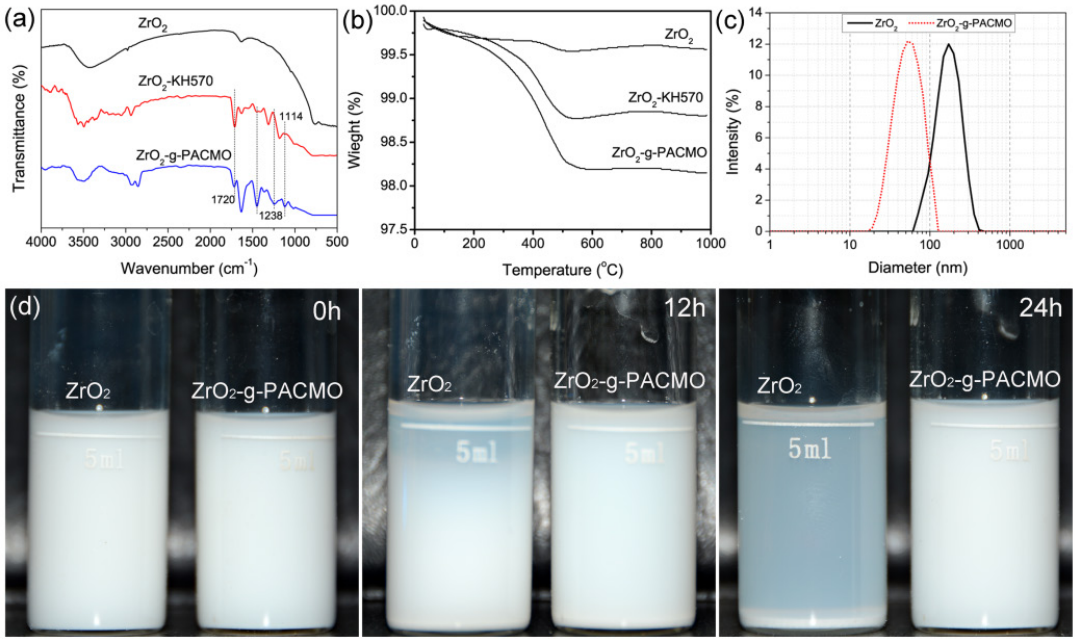

Fig. 1. (a) FTIR spectra and (b) TGA curves of ZrO_2, ZrO_2-KH570 and ZrO_2-*g*-PACMO nanoparticles; (c) particle size distributions and (d) sedimentation behaviors of ZrO_2 and ZrO_2-*g*-PACMO nanoparticles in DMF.

mass percentage of grafted PACMO chains is about 0.68 wt% of ZrO_2-KH570 nanoparticles weight. Therefore, the grafting amount of PACMO chains is about 0.05 mmol/g, as calculated by Eq. (9).

$$\text{Grafting amount}_{\text{PACMO}}\left(\text{mmol/g}\right)=\frac{W_2-\left(1-W_2\right)\times W_1}{M_{\text{ACMO}}}\times 10^3 \quad (9)$$

where W_1 and W_2 are the weight loss of ZrO_2-KH570 and ZrO_2-*g*-PACMO nanoparticles, respectively. $(1 - W_2) \times W_1$ represents the relative amount of KH570 onto ZrO_2 nanoparticles, and M_{ACMO} is the molecular weight of ACMO monomer.

To investigate the effect of the grafted PACMO chains on the agglomeration of ZrO_2 nanoparticles, the particle size distributions of nanoparticles were measured using DMF as the dispersant, and the results are shown in Fig. 1(c). It is found that the distribution of ZrO_2-*g*-PACMO nanoparticles has a narrower range, and the diameter is smaller than that of the original ZrO_2 nanoparticles. The mean diameter decreases from 210 to 65 nm, which is close to the diameter of original ZrO_2 nanoparticles (50 nm). This result shows that the agglomeration tendency of ZrO_2 nanoparticles is significantly suppressed via the grafting of PACMO chains.

The dispersion stability of nanoparticles was also studied via the sedimentation behavior in the organic solvent DMF. Xu et al. [41] reported there were two types of sedimentation mechanisms of nanoparticles, such as flocculation and accumulation. As shown in Fig. 1(d), the original ZrO_2 nanoparticles are accumulated at the bottom, while column of cloudy supernatant suspension still remains after settling of 24 h. This sedimentation of ZrO_2 nanoparticles is typical for accumulation suspensions. In contrast, solution containing ZrO_2-*g*-PACMO nanoparticles exhibits the most turbidity. The appropriate reason should be attributed to the fact that the PACMO chains strengthen the interfacial stability of nanoparticles, which may be counter balanced by Brownian motion [42]. As a result, ZrO_2-*g*-PACMO nanoparticles remain in the supernatant for long times. Even after 24 h the solution containing ZrO_2-*g*-PACMO nanoparticles is still turbid. This result also confirms that the grafted PACMO chains can significantly increase the dispersion stability of nanoparticles in the organic solvent DMF. Since DMF is a good solvent for the PVC membrane formation, the uniform dispersion of ZrO_2-*g*-PACMO nanoparticles in the membrane matrix is expected.

3.2. Chemical structure of membranes

PVC, PVC/ZrO_2 and PVC/ZrO_2-*g*-PACMO membranes were fabricated via the phase inversion method. The surface chemistry of the prepared membranes was investigated by XPS. As depicted in Fig. 2, typical emissions of PVC can be observed at 201.3 eV for Cl2p and 286.1 eV for C1s [14]. There are two peaks at 532.8 and 181.1 eV, corresponding to O1s and Zr3d in the spectrum of PVC/ZrO_2 membrane, respectively [43]. As for the spectrum of ZrO_2-*g*-PACMO membrane, the N1s peak at 400.3 eV is certainly attributable to the grafted PACMO chains, indicating the presence of ZrO_2-*g*-PACMO nanoparticles in the PVC/ZrO_2-*g*-PACMO membrane [36]. The mole percentage of N is 3.47 mol%, which is termed as experimental value. Correspondingly, the calculated value of N is 0.036 mol% that is derived from molecular structures and concentrations of PVC polymer and ZrO_2-*g*-PACMO nanoparticle in the casting solution. Obviously, the experimental value of N elemental concentration is much higher than calculated value. This result shows that the hydrophilic PACMO chains prefer to migrate toward the membrane surfaces during membrane formation. This significant segregation of PACMO chains will substantially increase the surface hydrophilicity and protein fouling resistance of the prepared membranes [44].

3.3. Morphology of membranes

The cross-sectional and surface morphologies of the prepared membranes were observed by SEM. As shown in Fig. 3 (left and middle columns), the original PVC membrane shows a dense surface morphology, while the microporous structures are clearly observed on the surfaces of PVC/ZrO_2 and PVC/ZrO_2-*g*-PACMO membranes. The cross-section of the prepared PVC membrane presents a typical asymmetric structure consisting of a skin layer and a finger-like sub-layer. The PVC/ZrO_2 and PVC/ZrO_2-*g*-PACMO membranes exhibit a morphological change of sub-layer, in which the finger-like sub-layer transforms into the macrovoid. To investigate the mechanism of membrane formation, the viscosity of casting solutions was measured. It is found from Table 1 that the viscosity of casting solutions deceases after the nanoparticles are incorporated into the dope solution. The low viscosity of the casting solution accelerates the exchange rate of solvent and non-solvent during membrane formation, and a faster instantaneous liquid–liquid phase separation occurs,

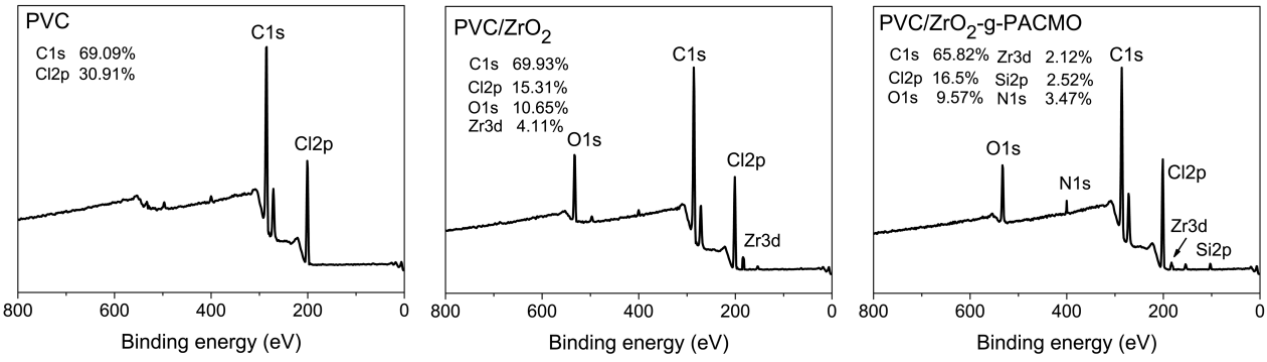

Fig. 2. Wide-scan XPS spectra of the original PVC, PVC/ZrO_2 and PVC/ZrO_2-*g*-PACMO membranes.

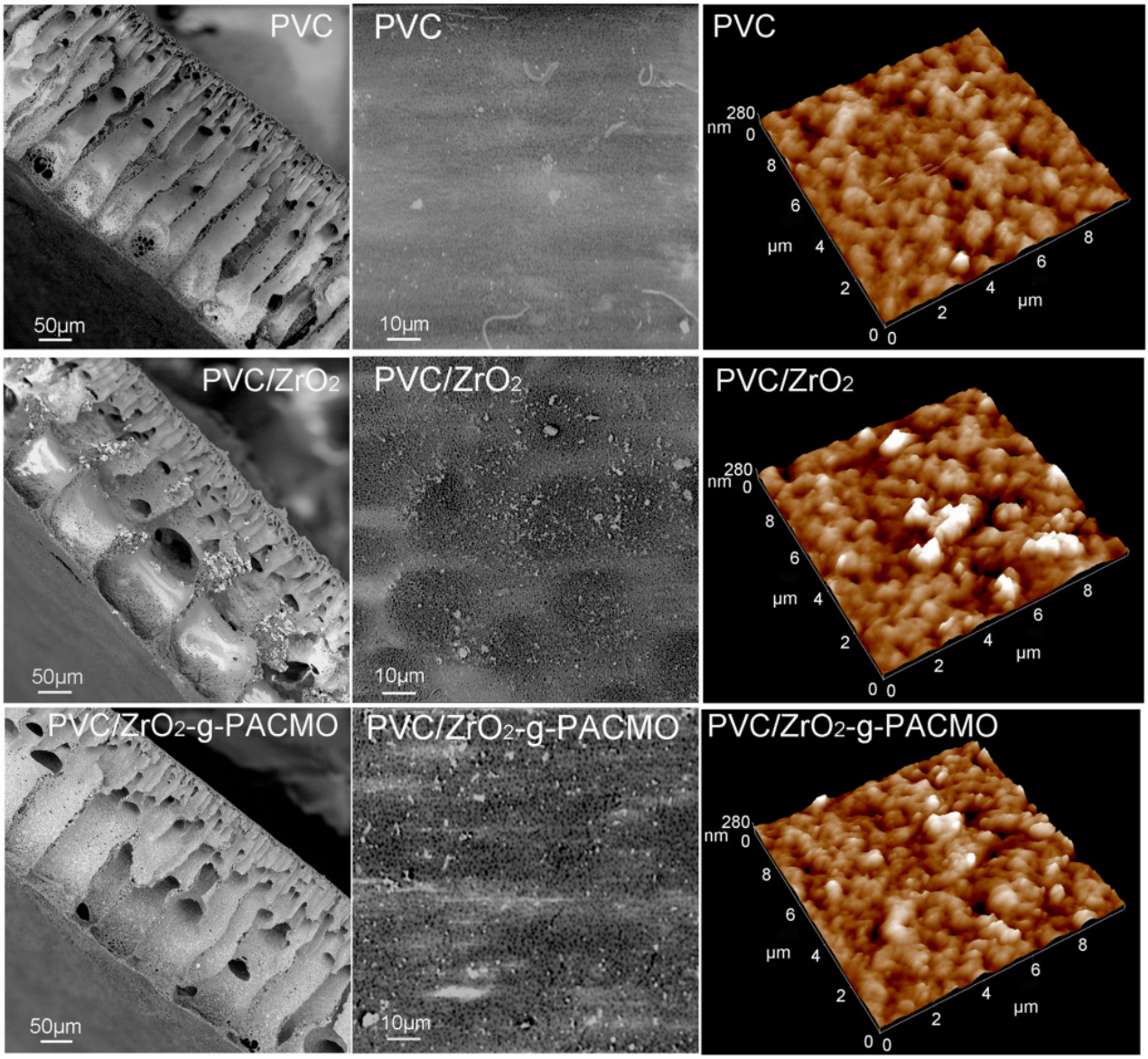

Fig. 3. Morphologies of original PVC, PVC/ZrO_2 and PVC/ZrO_2-*g*-PACMO membranes. Left column: cross-section of membranes; middle column: SEM images of membrane surfaces; right column: three-dimensional AFM images of membrane surfaces.

resulting in a porous surface and macroviod in the sub-layer [45]. Furthermore, the size of macrovoids at the cross-section of PVC/ZrO_2 membrane is higher than that of PVC/ZrO_2-*g*-PACMO membrane, which may be ascribed to the fact that the grafted PACMO chains significantly enhance the compatibility between nanoparticles and PVC polymer. Similar experimental results were also obtained previously by Zhang et al. [29] for the polysulfone hybrid membranes prepared from TiO_2 and TiO_2-*graft*-poly(hydroxyethyl methacrylate) (TiO_2-*g*-PHEMA) nanoparticles [29]. It is also observed from Fig. 3 that the ZrO_2 nanoparticles are aggregated at the center of PVC/ZrO_2 membrane. On the other hand, the typical aggregation of ZrO_2-*g*-PACMO is not displayed at the cross-section of PVC/ZrO_2-*g*-PACMO. This result indicates that the ZrO_2-*g*-PACMO nanoparticles are uniformly dispersed in the membrane matrix during membrane formation.

To qualitatively inspect the surface structure of membranes, the surface roughness parameters were determined via AFM system. As shown in Table 2 and Fig. 3 (right column), the surface roughness parameters of original PVC membrane are less than those of PVC/ZrO_2 and PVC/ZrO_2-*g*-PACMO membranes. The roughness parameters are strongly correlated to the depressions characterizing the pores and the high peaks characterizing the nodules. The high roughness parameters are expected when deep depressions and high peaks are presented on the membrane surface [46]. In the present work, the fast liquid–liquid phase separation is generated by the addition of ZrO_2 and ZrO_2-*g*-PACMO nanoparticles, which endows the prepared PVC/ZrO_2 and PVC/ZrO_2-*g*-PACMO membranes with the high surface pore size. Therefore, the surface morphologies of PVC/ZrO_2 and PVC/ZrO_2-*g*-PACMO membranes are rougher than that of original PVC membrane.

Table 2
Surface roughness parameters, porosity (ε) and mean pore size (d_m) of original PVC, PVC/ZrO_2 and PVC/ZrO_2-*g*-PACMO membranes

Membrane ID	R_a (nm)	R_q (nm)	R_z (nm)	ε (%)	d_m (nm)
PVC	25.0 ± 4.0	32.1 ± 5.4	261.5 ± 32.3	69.2 ± 1.4	10.7 ± 0.9
PVC/ZrO_2	27.9 ± 2.9	35.4 ± 2.9	282.0 ± 33.5	73.0 ± 1.1	25.6 ± 0.6
PVC/ZrO_2-*g*-PACMO	35.5 ± 7.0	43.6 ± 8.3	320.2 ± 26.6	76.5 ± 1.6	56.8 ± 1.3

Fig. 4 shows the pore size distributions of original PVC, PVC/ZrO_2 and PVC/ZrO_2-*g*-PACMO membranes, and the porosity and mean pore size of membranes are also summarized in Table 2. The curves of pore size distributions shift to the right, and the porosity and pore size of the membranes increase after ZrO_2 and ZrO_2-*g*-PACMO nanoparticles are introduced into the membranes. This result is well consistent with the morphologies of membranes, as revealed in Fig. 3. As reported by Arthanareeswaran et al. [47], the blending of hydrophilic nanoparticles in polymer matrix can increase the volume fraction among the polymer chains. Together with the fast exchange of solvent and non-solvent during the phase inversion process, the porosity and mean pore size of the prepared membranes increase. Interestingly, the mean pore size of membranes seems much smaller than surface pore size observed in AFM images in Fig. 3. The difference may be explained that only size in the range of 2–100 nm can be measured in the adsorption–desorption experiments [34].

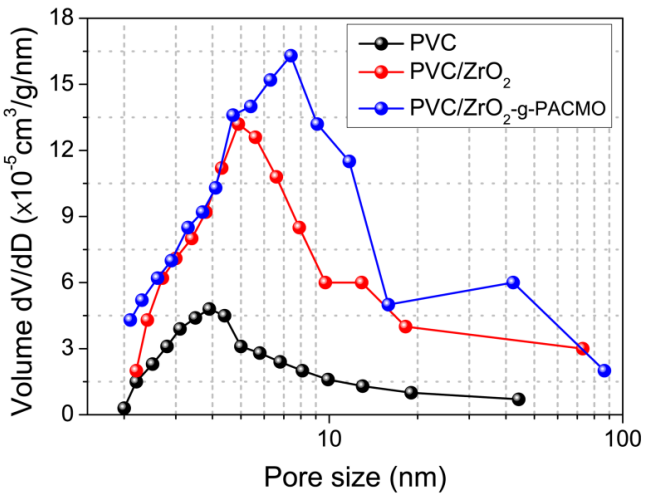

Fig. 4. Pore size distributions of original PVC, PVC/ZrO_2 and PVC/ZrO_2-*g*-PACMO membranes.

3.4. Anti-fouling property of membranes

Water contact angle measurements were utilized to evaluate the surface hydrophilicity of the prepared membranes. As shown in Fig. 5(a), the original PVC membrane exhibits a maximum initial contact angle of 94.5°, indicating the hydrophobic nature of PVC. The contact angles of PVC/ZrO_2 and PVC/ZrO_2-*g*-PACMO are smaller than that of PVC membrane. Especially for PVC/ZrO_2-*g*-PACMO membrane, the initial contact angle is 70.6° that is 23.9° decrease comparing with original PVC membrane. Furthermore, the decay propensity of the dynamic contact angle is observed on the PVC/ZrO_2 and PVC/ZrO_2-*g*-PACMO membrane surface. The values decrease from 80.4° to 60.2° for PVC/ZrO_2 membrane, and from 70.6° to 49.2° for PVC/ZrO_2-*g*-PACMO membrane, respectively. However, the contact angle of the original PVC membrane remains stable during the drop age (80 s). The decay rate of contact angle is always affected by the hydrophilicity of the membrane surface, the surface pore size and wettability of internal pore channel surface [48]. The PACMO chains are easily segregated onto the membrane surface and pore channel surface during membrane formation. When a water droplet is contacted with the membrane surface, the hydrogen bonds between the PACMO and the water molecules result in an instant spreadability [34,35]. These results suggest that the PVC/ZrO_2-*g*-PACMO membrane is more hydrophilic than PVC/ZrO_2 and original PVC membrane.

The fouling resistance of membranes was evaluated via the protein adsorption measurements. The fouling test results for the prepared membranes are shown in Fig. 5(b). The amount of adsorbed BSA on PVC membrane is 278 μg/cm², which is substantially higher than 151 μg/cm² of PVC/ZrO_2 and 78 μg/cm² of PVC/ZrO_2-*g*-PACMO membranes. This result indicates that the original PVC membrane is easily fouled by the protein adsorption. Compared with original ZrO_2 nanoparticles, ZrO_2-*g*-PACMO is more conducive to improve the fouling resistance of PVC membrane.

To further survey the anti-fouling mechanisms of membranes, the interaction force between BSA-immobilized AFM tip and membrane surface was measured [38]. As shown in Fig. 6, the interaction force between the original PVC membrane and BSA-immobilized tip is about 23.6 nN. The interaction force decreases to 18.7 and 12.2 nN, corresponding to PVC/ZrO_2 and PVC/ZrO_2-*g*-PACMO membranes, respectively. With respect to the adsorbed BSA amounts of membranes, it is obvious that, the weaker the adhesion force of the membrane-BSA, the lower amounts of protein adsorption.

It is well known that the rough membrane surface easily adsorbs foulants from an aqueous media. The stronger anti-fouling ability of membranes is always generated from a smoother surface [49]. In the present work, although the PVC/ZrO_2-*g*-PACMO membrane surface is coarser than PVC/ZrO_2 and original PVC membranes, PVC/ZrO_2-*g*-PACMO membrane performs better to resist protein adsorption. The improved surface hydrophilicity is one of the dominated factors affecting the anti-fouling ability of the membrane. Water molecules are integrated with PACMO chains to form a hydrated membrane surface [36]. The strong hydration ability of PACMO remarkably decreases the interaction force between the protein and membrane surface, and then effectively resists the protein to adsorb onto PVC/ZrO_2-*g*-PACMO membrane.

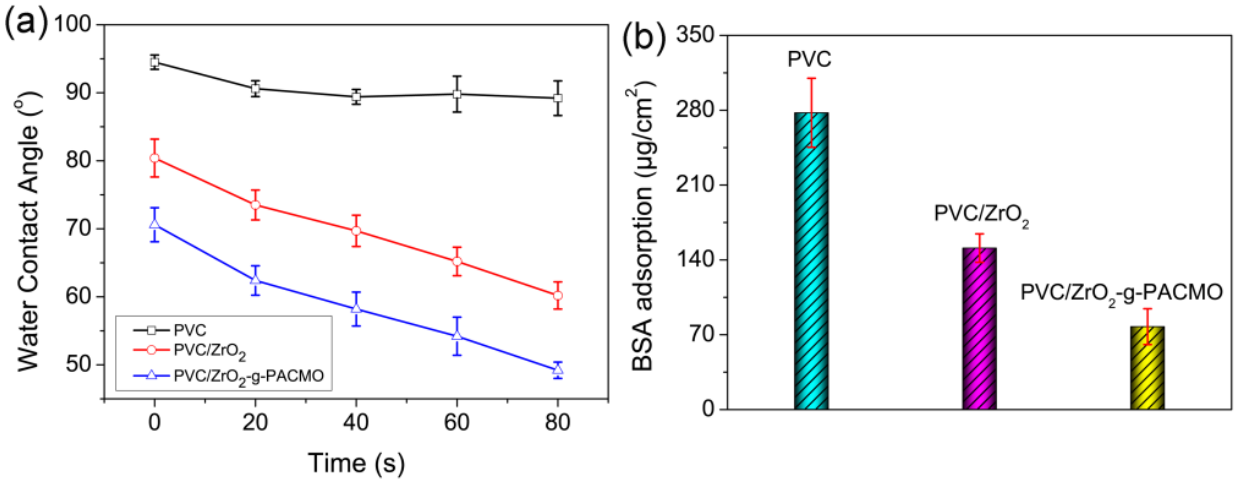

Fig. 5. (a) Water contact angles and (b) adsorbed BSA amounts of original PVC, PVC/ZrO_2 and PVC/ZrO_2-*g*-PACMO membranes.

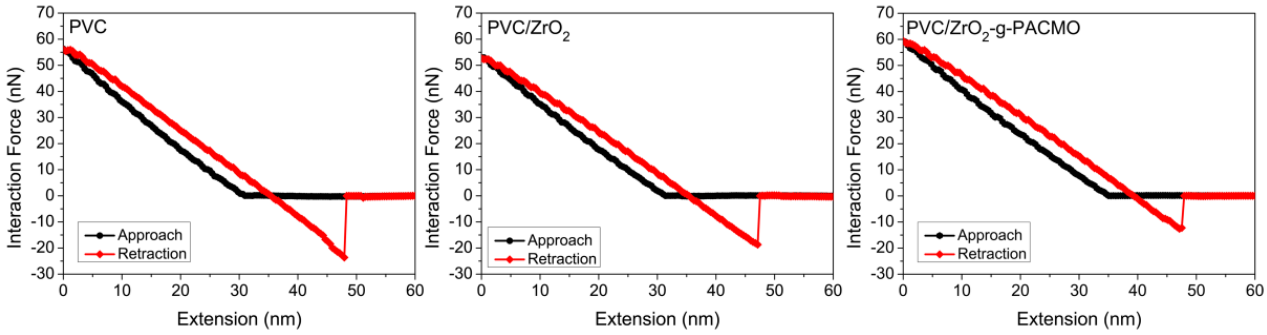

Fig. 6. Force-extension curves recorded with a BSA-immobilized tip against original PVC, PVC/ZrO_2 and PVC/ZrO_2-*g*-PACMO membranes.

3.5. Permeability of membranes

Cycle filtration was carried out to evaluate the permeability of original PVC, PVC/ZrO_2 and PVC/ZrO_2-*g*-PACMO membranes. The filtration process included three steps: the pure water filtration, filtration of BSA solution (0.5 g/L) and pure water filtration after membrane was cleaned with water for 30 min. The fluxes in each stage were calculated, which were termed as $J_{w,1}$, J_p and $J_{w,2}$ respectively. As depicted in Fig. 7 and Table 3, the fluxes of membranes increase, whereas the rejection ratios of BSA decrease after the addition of ZrO_2 and ZrO_2-*g*-PACMO into the membrane. This phenomenon may be the synthetic effects of surface hydrophilicity and membrane structures [50]. The improved hydrophilicity of membranes favorably accelerates the transportation of water molecules. On the other hand, the incorporation of ZrO_2 and ZrO_2-*g*-PACMO nanoparticles renders the membrane with a high pore size and porosity, which also allows the water and BSA molecules to permeate through the membrane matrix.

The FR can obviously present the suitable recycling performance of the PVC/ZrO_2-*g*-PACMO membrane. The higher FR implies a better anti-fouling property for the membrane [16]. From Table 3, the FR of the original PVC membrane is about 32.2%, suggesting that the serious flux decline is generated from the BSA adsorption. More importantly, the FR

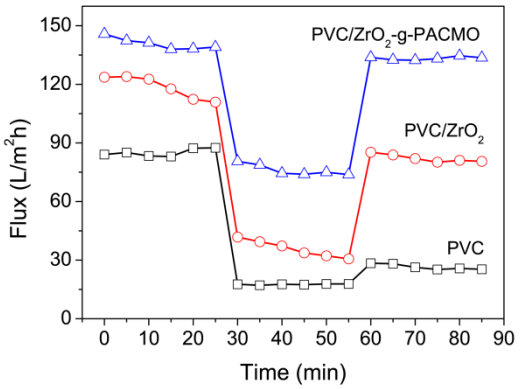

Fig. 7. Time-dependent fluxes of original PVC, PVC/ZrO_2 and PVC/ZrO_2-*g*-PACMO membranes.

value PVC/ZrO_2-*g*-PACMO membrane is as high as 94.7%. This is resulted from the hydrophilic effect of grafted PACMO chains. Furthermore, the well-dispersed ZrO_2-*g*-PACMO in the membrane pore channel makes the entrapped BSA in the pores to be removed easily by water flushing. The result indicates that the prepared PVC/ZrO_2-*g*-PACMO membrane

Table 3
Fouling ratio, flux recovery and BSA rejection of PVC, PVC/ZrO_2 and PVC/ZrO_2-*g*-PACMO membranes

Membrane ID	R_r (%)	R_{ir} (%)	R_t (%)	FR (%)	Rejection (%)
PVC	10.5	68.8	79.3	31.2	62.4 ± 5.2
PVC/ZrO_2	39.1	30.7	69.8	69.3	41.3 ± 4.6
PVC/ZrO_2-*g*-PACMO	40.7	5.3	46.0	94.7	27.6 ± 3.8

shows the better anti-fouling property than PVC membrane. Recently, Behboudi et al. [23] reported that the FR value of PVC/TiO_2 membrane was 97.6% when 2 wt% of TiO_2 nanoparticles was added in the casting solution. Also, Rabiee et al. [21] found that FR value of the prepared PVC/ZnO reached to 95.6% at 3 wt% of ZnO nanoparticle concentration. The FR of the prepared PVC/ZrO_2-*g*-PACMO membrane (94.7%) is closed to the excremental results of abovementioned hybrid membranes. In the present work, it is noteworthy that the concentration of added ZrO_2-*g*-PACMO is smaller than those of ZnO and TiO_2 nanoparticles in PVC membrane. The result also demonstrates that the synthesized ZrO_2-*g*-PACMO performs better to improve the anti-fouling property of PVC membrane, as compared with ZnO and TiO_2 nanoparticles.

To quantitatively analyze the protein fouling resistance of membrane in detail, the reversible fouling ratio (R_r), the irreversible ratio (R_{ir}) and total fouling ratio (R_t) were calculated. The results are also given in Table 3. As the hydrophobic interactions between the PVC membrane surface and BSA, the R_{ir} value of PVC membrane is 68.8%, about 86.8% of total fouling. However, after ZrO_2 and ZrO_2-*g*-PACMO are introduced into the membranes, the R_{ir} values remarkably decease. Especially for the PVC/ZrO_2-*g*-PACMO membrane, the R_{ir} value is only 11.5% of total fouling ratio. This result indicates that the incorporation of ZrO_2-*g*-PACMO can suppress the irreversible adhesion of BSA protein on the membrane surface. The PACMO chains are integrated with water molecules to form a stable hydration layer, which prevents the irreversible adhesion of protein molecules on the membrane surface [48]. On the other hand, although the reversible adhesion of BSA protein is generated, the FR of PVC/ZrO_2-*g*-PACMO still reaches to 94.7%, since the reversible fouling can be mitigated via a simple water flushing [50].

4. Conclusions

The PACMO-grafted ZrO_2 nanoparticles (ZrO_2-*g*-PACMO) were directly blended with PVC to prepare PVC/ZrO_2-*g*-PACMO membrane via phase inversion method. The ZrO_2-*g*-PACMO nanoparticles were well dispersed in DMF that was the good solvent for PVC. The addition of ZrO_2 and ZrO_2-*g*-PACMO nanoparticles rendered the prepared membrane with the macroviod of cross-section and a rough membrane surface. The hydrophilic PACMO chains were preferably segregated on the membrane surface and pore channel surface during the membrane formation, resulting in the increase of surface hydrophilicity and the decrease of interaction force between protein and membrane surface. Therefore, the prepared PVC/ZrO_2-*g*-PACMO membrane exhibited smaller protein adsorption than those of original PVC and PVC/ZrO_2 membranes. The filtration experiments indicated that the irreversible protein adhesion of PVC/ZrO_2-*g*-PACMO membrane was significantly mitigated. Although the PVC/ZrO_2 membrane also performed better to resist protein fouling as compared with original PVC membrane, the blending of ZrO_2 nanoparticles was still insufficient to improve anti-fouling property of PVC membrane because it had the agglomeration propensity during membrane formation. In fact, the physicochemical properties in terms of surface roughness, wettability and surface charge, are the factors affecting the anti-fouling ability of membrane. The effects of nanoparticles concentration on the structures, hydrophilicity and anti-fouling property of PVC membranes will be further investigated in our future works.

Acknowledgments

This research is financially supported by National Natural Science Foundation of China (Grant No. 51703118), Yunnan Applied Basic Research Projects of China (Grant No. 2015FD047) and Innovation Training Program of Chinese College Students (Grant No. 201610684007). The authors wish to acknowledge Prof. Li Chen and Prof. Yiping Zhao for membrane characterization at Tianjin Polytechnic University of China.

References

[1] F. Soyekwo, Q.G. Zhang, R.S. Gao, Y. Qu, C.X. Lin, X.L. Huang, A.M. Zhu, Q.L. Liu, Cellulose nanofiber intermediary to fabricate highly-permeable ultrathin nanofiltration membranes for fast water purification, J. Membr. Sci., 524 (2017) 174–185.
[2] A. Helling, A. Kubicka, I.A.T. Schaap, M. Polakovic, B. Hansmann, H. Thiess, J. Strube, V. Thom, Passage of soft pathogens through microfiltration membranes scales with transmembrane pressure, J. Membr. Sci., 522 (2017) 292–302.
[3] R.N. Zhang, Y.N. Liu, M.R. He, Y.L. Su, X.T. Zhao, M. Elimelech, Z.Y. Jiang, Antifouling membranes for sustainable water purification: strategies and mechanisms, Chem. Soc. Rev., 45 (2016) 5888–5924.
[4] H.L. Liu, C.F. Xiao, Q.L. Huang, X.Y. Hu, W. Shu, Preparation and interface structure study on dual-layer polyvinyl chloride matrix reinforced hollow fiber membranes, J. Membr. Sci., 472 (2014) 210–221.
[5] J. Chapman, A. Lawlor, E. Weir, B. Quilty, F. Regan, Phthalate doped PVC membranes for the inhibition of fouling, J. Membr. Sci., 365 (2010) 180–187.
[6] X.Z. Zhang, Y.S. Chen, A.H. Konsowa, X.S. Zhu, J.C. Crittenden, Evaluation of an innovative polyvinyl chloride (PVC) ultrafiltration membrane for wastewater treatment, Sep. Purif. Technol., 70 (2009) 71–78.
[7] S.M. Hosseini, S.S. Madaeni, A. Zendehnam, A.R. Moghadassi, A.R. Khodabakhshi, H. Sanaeepur, Preparation and characterization of PVC based heterogeneous ion exchange membrane coated with Ag nanoparticles by (thermal-plasma) treatment assisted surface modification, J. Ind. Eng. Chem., 19 (2013) 854–862.

[8] R. Patel, M. Patel, S.H. Ahn, Y.K. Sung, H.K. Lee, J.H. Kim, J.S. Sung, Bioinert membranes prepared from amphiphilic poly(vinyl chloride)-*g*-poly(oxyethylene methacrylate) graft copolymers, Mater. Sci. Eng., C, 33 (2013) 1662–1670.
[9] S. Rajabzadeh, R. Sano, T. Ishigami, Y. Kakihana, Y. Ohmukai, H. Matsuyama, Preparation of hydrophilic vinyl chloride copolymer hollow fiber membranes with antifouling properties, Appl. Surf. Sci., 324 (2015) 718–724.
[10] L.F. Fang, B.K. Zhu, L.P. Zhu, H. Matsuyama, S.F. Zhao, Structures and antifouling properties of polyvinyl chloride/poly(methyl methacrylate)-graft-poly(ethylene glycol) blend membranes formed in different coagulation media, J. Membr. Sci., 524 (2017) 235–244.
[11] Y.L. Su, Q. Zhao, J.Z. Liu, J.J. Zhao, Y.F. Li, Z.J. Jiang, Improved oil/water emulsion separation performance of PVC/CPVC blend ultrafiltration membranes by fluorination treatment, Desal. Wat. Treat., 55 (2015) 304–314.
[12] M.H.D.A. Farahani, H. Rabiee, V. Vatanpour, S.M. Borghei, Fouling reduction of emulsion polyvinylchloride ultrafiltration membranes blended by PEG: the effect of additive concentration and coagulation bath temperature, Desal. Wat. Treat., 57 (2016) 11931–11944.
[13] A. Behboudi, Y. Jafarzadeh, R. Yegani, Polyvinyl chloride/polycarbonate blend ultrafiltration membranes for water treatment, J. Membr. Sci., 534 (2017) 18–24.
[14] Z. Zhou, S. Rajabzadeh, A.R. Shaikh, Y. Kakihana, W.Z. Ma, H. Matsuyama, Effect of surface properties on antifouling performance of poly(vinyl chloride-*co*-poly(ethyleneglycol) methyl ether methacrylate)/PVC blend membrane, J. Membr. Sci., 514 (2016) 537–546.
[15] X. Shen, Y.P. Zhao, X. Feng, S.X. Bi, W.B. Ding, L. Chen, Improved antifouling properties of PVDF membranes modified with oppositely charged copolymer, Biofouling, 29 (2013) 331–343.
[16] B.C. Liu, C. Chen, W. Zhang, J. Crittenden, Y.S. Chen, Low-cost antifouling PVC ultrafiltration membrane fabrication with Pluronic F127: effect of additives on properties and performance, Desalination, 307 (2012) 26–33.
[17] A.L. Ahmad, A.A. Abdulkarim, Z.M.H. Mohd Shafie, B.S. Ooi, Fouling evaluation of PES/ZnO mixed matrix hollow fiber membrane, Desalination, 403 (2017) 53–63.
[18] S. Mei, C.F. Xiao, X.Y. Hu, W. Shu, Hydrolysis modification of PVC/PAN/SiO_2 composite hollow fiber membrane, Desalination, 280 (2011) 378–383.
[19] H.P. Xu, Y.H. Yu, W.Z. Lang, X. Yan, Y.J. Guo, Hydrophilic modification of polyvinyl chloride hollow fiber membranes by silica with a weak in situ sol–gel method, RSC Adv., 5 (2015) 13733–13742.
[20] L.C. Wang, Y.Y. Han, K.C. Yang, M.J. Chen, H.C. Lin, C.K. Lin, Y.T. Hsu, Hydrophilic/hydrophobic surface of Al_2O_3 thin films grown by thermal and plasma-enhanced atomic layer deposition on plasticized polyvinyl chloride (PVC), Surf. Coat. Technol., 305 (2016) 158–164.
[21] H. Rabiee, V. Vatanpour, M.H.D.A. Farahani, H. Zarrabi, Improvement in flux and antifouling properties of PVC ultrafiltration membranes by incorporation of zinc oxide (ZnO) nanoparticles, Sep. Purif. Technol., 156 (2015) 299–310.
[22] H. Rabiee, M.H.D.A. Farahani, V. Vatanpour, Preparation and characterization of emulsion poly(vinylchloride) (EPVC)/TiO_2 nanocomposite ultrafiltration membrane, J. Membr. Sci., 472 (2014) 185–193.
[23] A. Behboudi, Y. Jafarzadeh, R. Yegani, Preparation and characterization of TiO_2 embedded PVC ultrafiltration membranes, Chem. Eng. Res. Des., 114 (2016) 96–107.
[24] A. Razmjou, J. Mansouri, V. Chen, The effects of mechanical and chemical modification of TiO_2 nanoparticles on the surface chemistry, structure and fouling performance of PES ultrafiltration membranes, J. Membr. Sci., 378 (2011) 73–84.
[25] Y.J. Zhao, S.Y. Zhou, M.S. Li, A.L. Xue, Y. Zhang, J.G. Wang, W.H. Xing, Humic acid removal and easy-cleanability using temperature-responsive ZrO_2 tubular membranes grafted with poly(N-isopropylacrylamide) brush chains, Water Res., 47 (2013) 2375–2386.
[26] N. Maximous, G. Nakhla, W. Wan, K. Wong, Performance of a novel ZrO_2/PES membrane for wastewater filtration, J. Membr. Sci., 352 (2010) 222–230.
[27] Y.M. Zheng, S.W. Zou, K.G.N. Nanayakkara, T. Matsuura, J.P. Chen, Adsorptive removal of arsenic from aqueous solution by a PVDF/zirconia blend flat sheet membrane, J. Membr. Sci., 374 (2011) 1–11.
[28] J. Yin, J.C. Zhou, Novel polyethersulfone hybrid ultrafiltrationmembrane prepared with SiO_2-*g*-(PDMAEMA-*co*-PDMAPS) and its antifouling performances in oil-in-water emulsion application, Desalination, 365 (2015) 46–56.
[29] G.L. Zhang, S.F. Lu, L. Zhang, Q. Meng, C. Shen, J.W. Zhang, Novel polysulfone hybrid ultrafiltration membrane prepared with TiO_2-g-HEMA and its antifouling characteristics, J. Membr. Sci., 436 (2013) 163–173.
[30] L.F. Liu, H.P. Chen, F.L. Yang, Enhancing membrane performance by blending ATRP grafted PMMA–TiO_2 or PMMA–PSBMA–TiO_2 in PVDF, Sep. Purif. Technol., 133 (2014) 22–31.
[31] H. Takahashi, M. Nakayama, K. Itoga, M. Yamato, T. Okano, Micropatterned thermoresponsive polymer brush surfaces for fabricating cell sheets with well-controlled orientational structures, Biomacromolecules, 12 (2011) 1414–1418.
[32] W. Li, M. Nakayama, J. Akimoto, T. Okano, Effect of block compositions of amphiphilic block copolymers on the physicochemical properties of polymeric micelles, Polymer, 52 (2011) 3783–3790.
[33] C.L. Lo, S.J. Lin, H.C. Tsai, W.H. Chan, C.H. Tsai, C.H.D. Cheng, G.H. Hsiue, Mixed micelle systems formed from critical micelle concentration and temperature-sensitive diblock copolymers for doxorubicin delivery, Biomaterials, 30 (2009) 3961–3970.
[34] J. Liu, X. Shen, Y.P. Zhao, L. Chen, Acryloylmorpholine-grafted PVDF membrane with improved protein fouling resistance, Ind. Eng. Chem. Res., 52 (2013) 18392–18400.
[35] X. Shen, J. Liu, X. Feng, Y.P. Zhao, L. Chen, Preliminary investigation on hemocompatibility of poly(vinylidene fluoride) membrane grafted with acryloylmorpholine via ATRP, J. Biomed. Mater. Res. A, 103 (2015) 683–692.
[36] X. Shen, T.D. Xie, J.G. Wang, P. Liu, F. Wang, An anti-fouling poly(vinylidene fluoride) hybrid membrane blended with functionalized ZrO_2 nanoparticles for efficient oil/water separation, RSC Adv., 7 (2017) 5262–5271.
[37] L.J. Zhu, L.P. Zhu, Y.F. Zhao, B.K. Zhu, Y.Y. Xu, Anti-fouling and anti-bacterial polyethersulfone membranes quaternized from the additive of poly(2-dimethylamino ethyl methacrylate) grafted SiO_2 nanoparticles, J. Mater. Chem. A, 2 (2014) 15566–15574.
[38] J.G. Zhang, Z.W. Xu, W. Mai, C.Y. Min, B.M. Zhou, M.J. Shan, Y.L. Li, C.Y. Yang, Z. Wang, X.M. Qian, Improved hydrophilicity, permeability, antifouling and mechanical performance of PVDF composite ultrafiltration membranes tailored by oxidized low-dimensional carbon nanomaterials, J. Mater. Chem. A, 1 (2013) 3101–3111.
[39] E.C. Cho, D.H. Kim, K. Cho, Contact angles of oils on solid substrates in aqueous media: correlation with AFM data on protein adhesion, Langmuir, 24 (2008) 9974–9978.
[40] B.J. Gao, Y.X. Chen, Z.G. Zhang, Preparation of functional composite grafted particles PDMAEMA/SiO_2 and preliminarily study on functionality, Appl. Surf. Sci., 257 (2010) 254–260.
[41] X. Xu, M. Oliveira, J.M.F. Ferreira, Effect of solvent composition on dispersing ability of reaction sialon suspensions, J. Colloid Interface Sci., 259 (2003) 391–397.
[42] M. Sabzi, S.M. Mirabedini, J. Zohuriaan-Mehr, M. Atai, Surface modification of TiO_2 nano-particles with silane coupling agent and investigation of its effect on the properties of polyurethane composite coating, Prog. Org. Coat., 65 (2009) 222–228.
[43] R.Z. Pang, X. Li, J.S. Li, Z.Y. Lu, X.Y. Sun, L.J. Wang, Preparation and characterization of ZrO_2/PES hybrid ultrafiltration membrane with uniform ZrO_2 nanoparticles, Desalination, 332 (2014) 60–66.
[44] J. Zhu, X.Z. Zhao, C.J. He, Zwitterionic SiO_2 nanoparticles as novel additives to improve the antifouling properties of PVDF membranes, RSC Adv., 5 (2015) 53653–53659.

[45] Y.L. Zhang, J. Zhao, H.Q. Chu, X.F. Zhou, Y. Wei, Effect of modified attapulgite addition on the performance of a PVDF ultrafiltration membrane, Desalination, 344 (2014) 71–78.
[46] M. Khayet, M.C. García-Payo, F.A. Qusay, M.A. Zubaidy, Structural and performance studies of poly(vinyl chloride) hollow fiber membranes prepared at different air gap lengths, J. Membr. Sci., 330 (2009) 30–39.
[47] G. Arthanareeswaran, T.K.S. Devi, M. Raajenthiren, Effect of silica particles on cellulose acetate blend ultrafiltration membranes: part I, Sep. Purif. Technol., 64 (2008) 38–47.
[48] M.Z. Li, J.H. Li, X.S. Shao, J. Miao, J.B. Wang, Q.Q. Zhang, X.P. Xu, Grafting zwitterionic brush on the surface of PVDF membrane using physisorbed free radical grafting technique, J. Membr. Sci., 405–406 (2012) 141–148.
[49] Y. Wei, H.Q. Chu, B.Z. Dong, X. Li, S.J. Xia, Z.M. Qiang, Effect of TiO_2 nanowire addition on PVDF ultrafiltration membrane performance, Desalination, 272 (2011) 90–97.
[50] X. Shen, X.B. Yin, Y.P. Zhao, L. Chen, Antifouling enhancement of PVDF membrane tethered with polyampholyte hydrogel layers, Polym. Eng. Sci., 55 (2015) 1367–1373.